PHOTOSYNTHETICA
International Journal for Photosynthesis Research

DOI 10.32615/ps.2022.041 PHOTOSYNTHETICA 60 (4): 476-488, 2022

Improvement in the photoprotective capability benefits the productivity of a yellow-green wheat mutant in N-deficient conditions

X.H. ZHANG*, H.X. LI*, G. ZHUO*,**, Z.Z. HE*, C.Y. ZHANG*, Z. SHI*, C.C. LI*, and Y. WANG*,+

*College of Agronomy, Northwest A&F University, 712100 Yangling, Shaanxi, China**
*State Key Laboratory of Hulless Barley and Yak Germplasm Resources and Genetic Improvement, Lhasa, Tibet, China***

Abstract

Wheat yellow-green mutant *Jimai5265yg* has a more efficient photosynthetic system and higher productivity than its wild type under N-deficient conditions. To understand the relationship between photosynthetic properties and the grain yield, we conducted a field experiment under different N application levels. Compared to wild type, the *Jimai5265yg* flag leaves had higher mesophyll conductance, photosynthetic N-use efficiency, and photorespiration in the field without N application. Chlorophyll *a* fluorescence analysis showed that PSII was more sensitive to photoinhibition due to lower nonphotochemical quenching (NPQ) and higher nonregulated heat dissipation. In N-deficient condition, the PSI acceptor side of *Jimai5265yg* was less reduced. We proposed that the photoinhibited PSII protected PSI from over-reduction through downregulation of electron transport. PCA analysis also indicated that PSI photoprotection and electron transport regulation were closely associated with grain yield. Our results suggested that the photoprotection mechanism of PSI independent of NPQ was critical for crop productivity.

Keywords: nitrogen application rate; photoprotection; photosynthetic N-use efficiency; wheat; yellow-green mutant.

Highlights

- Photochemical efficiency of PSI and PSII was higher in the mutant without N application
- The mutant had a more efficient photoprotective mechanism for PSI independent of NPQ
- Regulation of electron transport is related to PSI photoprotection and grain yield

Received 10 February 2022
Accepted 18 August 2022
Published online 20 September 2022

+Corresponding author
e-mail: wangyucau@126.com

Abbreviations: C_c – CO_2 concentration inside the chloroplast; C_i – intercellular CO_2 concentration; ETRI – electron transport rate of PSI; ETRII – electron transport rate of PSII; F_0 – minimum fluorescence; F_0'– minimum fluorescence in the actinic light; F_m – maximum fluorescence; F_m' – maximum fluorescence in the actinic light; F_v/F_m – maximum quantum efficiency of PSII photochemistry; g_m – mesophyll conductance; g_s – stomatal conductance; J_a – alternative electron flux; $J_{e(PCO)}$ – electron flux to photorespiratory carbon oxidation; $J_{e(PCR)}$ – electron flux to photosynthetic carbon reduction; J_{max} – light-saturated potential rate of electron transport; J_t – electron transport rate; L_b – limitation of biochemical capacity; L_m – limitation of mesophyll diffusion; LMA – leaf mass per area; L_s – limitation of stomatal diffusion; N_{area} – nitrogen content per unit area; N_{mass} – nitrogen content per unit mass; NO – nonregulated heat dissipation; NPQ – nonphotochemical quenching; P700 – primary electron donor of PSI; PIB – post-illumination burst; P_m or P_m' – maximum P700 signal measured using saturation light pulse following short far-red pre-illumination in dark or light-adapted state; P_N – net photosynthetic rate; PNUE – photosynthetic N-use efficiency; q_P – PSII efficiency factor (the fraction of open centers); R_d – mitochondrial CO_2 release in the dark; R_L – light respiration rate; ROS – reactive oxygen species; $V_{c,max}$ – maximum carboxylation rate limited by Rubisco; Γ* – CO_2-compensation point; Φ_{NA} – oxidation status of PSI acceptor site; Φ_{ND} – oxidation status of PSI donor site; Φ_{NO} – quantum yield nonregulated heat dissipation; Φ_{NPQ} – quantum yield of nonphotochemical quenching; Φ_{PSI} – quantum yield of PSI photochemistry; Φ_{PSII} – PSII operating efficiency (quantum yield of PSII photochemistry); Φ_{qP} – quantum yield of open centers.

Acknowledgements: This work was supported by the National Natural Science Foundation of China (grant no. 31871618), Natural Science Foundation Research Program of Shaanxi Province (grant no. 2018JQ3062), National Key Research and Development Plan (grant no. 2017YFD0100706), Key Research and Development Program of Shaanxi Province (2021NY-082).
Conflict of interest: The authors declare that they have no conflict of interest.

Introduction

Nitrogen fertilizer is an essential factor for wheat production by influencing organ development and photosynthetic efficiency. A large amount of N is invested in the photosynthetic apparatus. Insufficient N application often leads to downregulation of photosynthesis (Byeon *et al.* 2021), while nitrogen fertilizer overapplication results in environmental costs and lowered nitrogen-use efficiencies (Tian *et al.* 2018). It has been reported that the rice cultivar with higher nitrogen-use efficiency had better photosynthetic performance (Kumari *et al.* 2021). Photosynthetic capacity is highly influenced by leaf structure and components in the chloroplasts, which were related to leaf N content regulated by N application. Evaluation of photosynthetic properties of germplasms with diverse chloroplast components under different levels of N supply was a way to understand the relationship between leaf photosynthesis and nitrogen, which was a fundamental production–resource function for ecosystem functioning (Rotundo and Cipriotti 2017). Also, the selection of germplasms insensitive to low N application is a strategy for improving N utilization and sustainable agricultural development.

The photosynthetic structural components of the light reactions are genetically conserved and have a less natural genetic variation (Nunes-Nesi *et al.* 2016). However, many mutants in Chl content and antenna sizes have been identified indicating higher natural genetic variation. Ort suggested that optimizing light antenna size could serve as a potential engineering target (Ort *et al.* 2011, Nunes-Nesi *et al.* 2016). Recent research on global atmospheric changes showed that solar irradiance on the Earth's surface increased due to reduced atmospheric aerosol. Mutants with reduced leaf Chl content provided an effective solution to mitigate the high solar irradiance (Genesio *et al.* 2021). The Chl-less mutants of different crops, such as rice, wheat, maize, and soybean, have been studied. It is reasonable that the photosynthetic rate of Chl-deficient mutants is reduced due to the restricted light-harvesting complex (Terao and Katoh 1996). However, a typical study using soybean pale-green mutant *Y11y11* showed that the photosynthetic efficiency and biomass accumulation were unaffected by the reduction of Chl content (Walker *et al.* 2018). Likewise, another soybean mutant (*y9y9*), rice mutant (*yg1*), *Arabidopsis thaliana* mutant (*dLhcb2*, *hpe1*), and cotton mutant (*virescent*) showed normal or higher photosynthetic capability compared to the corresponding wild type (Benedict *et al.* 1972, Li *et al.* 2013, Jin *et al.* 2016, Sakowska *et al.* 2018, Bielczynski *et al.* 2020).

Why is there such a counter-intuitive relationship between Chl content and photosynthetic rate? Studies using the above mutants provided four pieces of evidence and reasonings. Firstly, Chl-deficiency enables a more even distribution of sunlight within a crop canopy in the field. In the Chl-less population, a more significant fraction of light penetrated the lower leaves where the light was limiting and decreased the saturation of the upper leaves (Ort *et al.* 2015). Secondly, the Chl-deficient mutant has a more even light distribution among chloroplasts within leaves (Slattery and Ort 2021). Gradient light distribution within leaves restrains the function of chloroplasts buried in the lower part of the leaf. Photosynthetic efficiency in the lower chloroplasts increased by achieving more light in the Chl-less mutants. Thirdly, the absorbed light energy conversion efficiency improved in the Chl-less mutant. It has been documented that light energy absorbed by the Chl antennas excessed the efficiency of photochemistry, resulting in the generation of reactive oxygen species (ROS) and dissipation as NPQ and heat (Ort *et al.* 2011). The process of photoprotection of PSII and PSI consumed the absorbed light energy that could otherwise be used for carbon assimilation (Slattery and Ort 2021). Fourthly, Chl-deficient mutants exhibited improved photosynthetic N-use efficiency (PNUE) (Gu *et al.* 2017). Excessive Chl in large light antenna complex was inactive and occupied abundant leaf N. Chl-deficient mutants optimized leaf N-use by investing more N into carboxylation and substrate regeneration processes (Genesio *et al.* 2021).

Our previous study characterized a yellow-green wheat mutant *Jimai5265yg* during tissue culture. Genetic analysis indicated that the trait of less Chl was controlled by recessive gene loci on chromosome 4. The mutant had a higher quantum yield of PSII photochemistry (Φ_{PSII}) and mesophyll conductance (g_m), which contributed to the improved photosynthetic efficiency. Furthermore, the photosynthetic advantage was maintained in response to the N-deficient treatment in hydroponic culture. In addition to the enhanced CO_2 diffusion, the N-deficient mutant has a higher cyclic electron transport and photochemical activity of PSI, coping with photodamage (Li *et al.* 2021). N deficiency induced the increase of relative N content of the photosynthetic system in both wheat and rice (Hou *et al.* 2019). The higher PNUE of the N-deficient mutant could be attributed to the more optimal N-partitioning pattern within leaves. The biomass and yield of the Chl-deficient mutants slightly declined by the pleiotropic effect of genetic mutation (Genesio *et al.* 2021). However, the grain yield of *Jimai5265yg* increased by 18% compared to the wild type in the field without N application (Table 1S, *supplement*). Other agronomic traits, such as spike number and 1,000-grain mass did not exhibit a significant difference between the two genotypes. The grain number per spike rather than the other two yield components (thousand kernel mass and spike number) was the dominant contribution to the higher yield (Zheng *et al.* 2021). What are the differences in photosynthetic parameters between two genotypes in different N application levels at anthesis? Is there any relationship between photosynthetic properties and the increasing productivity for the mutant in the conditions without N application? Uncovering those problems might increase light-use efficiency and productivity through the genetic manipulation of the photosynthetic system.

In this study, we focused on the photosynthetic property of *Jimai5265yg* under different N-application conditions in the field at anthesis. Similar to the results of Zheng *et al.* (2021), N has little effect on the net

photosynthetic rate (P_N) in two genotypes. *Jimai5265yg* did not show apparent advantages over the wild type on P_N in the conditions without N application. However, PNUE and photorespiration of the mutant were higher. It has been reported that crop productivity was associated with the photoprotective mechanism (Kromdijk *et al.* 2016). So, we detected the PSI and PSII performance using chlorophyll *a* fluorescence. Despite the lower NPQ, the quantum yield of PSII and PSI chemistry in the mutant was higher in the conditions without N application. Though the photoinhibition of PSII was sensitive to N deficiency, the reduction level of PSI and PSII electron acceptors decreased. We suggested that the photoprotection of PSI and electron transport regulation might be associated with the higher grain yield of the mutant in the N-deficient conditions.

Materials and methods

Plant material and growth conditions: Wheat (*Triticum aestivum* L.) Jimai5265 and *Jimai5265yg* were used as experimental materials. According to the earlier study, the yellow-green mutant *Jimai5265yg* is a mutant line of wheat cultivar Jimai5265 with two chlorine mutations on chromosomes 4A and 4B (Wang *et al.* 2018). The mutant plants are yellow-green throughout the life span in the field.

The field N treatments were conducted at the reach farm (34°20'N, 108°24'E) of Northwest A&F University, Shaanxi Province, China. The altitude is 466.7 m, and soil composition is 36.5% clay, 61.1% silt, and 2.4% sand, pH of 8.4. The contents of soil organic matter, total nitrogen, total phosphorus, and total potassium were 13.09, 0.86, 0.71, and 14.76 g kg^{-1}, respectively, and the contents of available nitrogen, available phosphorus, and available potassium were 52.32 g kg^{-1}, 7.56 g kg^{-1}, and 187.06 mg kg^{-1}, respectively. The annual average temperature is 12.9°C, and the frost-free period is 211 d. The annual total solar radiation is 48.057 J m^{-2}, the annual sunshine duration is 2,163.8 h, and the average precipitation is 635.1 mm. The climate type is warm temperate semi-humid semi-arid climate. The trial was conducted from October 2018 to July 2019.

It was a complete randomized block field experiment with four N concentrations [N_0: 0 kg ha^{-1}, N_{120}: 120 kg ha^{-1}, N_{240}: 240 kg ha^{-1}, N_{360}: 360 kg ha^{-1}] for Jimai5265 and *Jimai5265yg*, respectively, and three replicates were set for each level. Each plot with an area of 9 m^2 (3 × 3 m) was separated by an isolated blank line of 30 cm. Calcium superphosphate (P_2O_5: 16%, 120 kg ha^{-1}) was applied as basal fertilizer. Nitrogen fertilizer was applied as urea (N ≥ 46%) before sowing. Wheat was artificially sowed on 3 October 2018, at a planting density of 150 kg ha^{-1}.

Flag leaf area, mass, and nitrogen content: Three representative wheat plants were randomly selected from each plot, and the whole flag leaves were cut. The cut leaves were fixed on the cardboard and scanned, and the flag leaf area was measured with *ImageJ 1.53* software.

The flag leaves were treated at 105°C for 30 min and dried at 80°C for 12 h to determine the dry mass. The flag leaves dried to constant mass were cut into pieces and transferred into a desiccating tube. The nitrogen content of the leaves was digested with H_2SO_4–H_2O_2 and determined using the flow analyzer (*AutoAnalyzer 3*, Germany).

Chlorophyll *a* fluorescence (CF) measurement: Chlorophyll *a* fluorescence of the flag leaves was measured using the *Dual-PAM-100* (*Heinz Walz GmbH*, Germany) from 6 to 8 May 2019 from 9:00–12:00 and 15:00–18:00 h. The parameters F_0, F_m, and P700 were determined after 30-min darkness adaptation. F_m' and F_s were measured after continuous illumination with an actinic light of 1,300 μmol(photon) m^{-2} s^{-1}. F_0', Φ_{PSII}, q_P, Φ_{NPQ}, Φ_{NO}, NPQ, and Φ_{qP} were calculated according to Oxborough and Baker (1997) and Kramer *et al.* (2004). Flag leaves of four individuals were measured for each genotype. A light curve was determined at a gradient of PAR [17, 58, 131, 213, 329, 500, 758; 1,177; 1,808; 2,804 μmol(photon) m^{-2} s^{-1}]. $F_0' = F_0/(F_v/F_m + F_0/F_m')$; $F_v/F_m = (F_m - F_0)/F_m$; $\Phi_{qP} = (F_m' - F_0')/F_m'$, $\Phi_{PSII} = (F_m' - F_s)/F_m'$; $q_P = (F_m' - F_s)/(F_m' - F_0')$; $NPQ = (F_m - F_m')/F_m'$; $q_L = q_P(F_0'/F_s)$; $\Phi_{NO} = 1/[NPQ + 1 + q_L(F_m/F_0 - 1)]$; $\Phi_{NPQ} = 1 - \Phi_{PSII} - \Phi_{NO}$; $\Phi_{PSI} = (P_m' - P)/P_m$; $\Phi_{ND} = P/P_m$; $\Phi_{NA} = (P_m - P_m')/P_m$.

Gas-exchange measurements: At anthesis, the flag leaf gas exchange was measured using the *Li-Cor 6400* portable photosynthesis system (*LI-COR*, *Inc.*). Three individuals of each genotype were measured. All measurements were made at a leaf temperature of 25°C and an air relative humidity of 40–60%. The CO_2-response curve (P_N/C_i) was determined under a series of reference CO_2 concentrations (400, 300, 200, 100, 50, 400, 600, 800, 1,000; 1,200; 1,500; 1,800 μmol mol^{-1}), while keeping PAR at 1,300 μmol(photon) m^{-2} s^{-1}. Post-illumination burst (PIB) measurements were taken after light adaption when CO_2 concentration was 400 μmol mol^{-1}. The lamps of the assimilation chamber were rapidly switched off and recorded automatically every second for 150 s. The absolute value of the minimum photosynthetic rate was PIB, and the absolute steady-state value of the photosynthetic rate was R_L (Ayub *et al.* 2011).

The maximum carboxylation rate limited by Rubisco ($V_{c,max}$), RuBP generation (J_{max}), CO_2 concentration inside the chloroplast (C_c), and CO_2-compensation point (Γ*) were calculated using the *R* package developed by Duursma and Remko based on the model of Farquhar *et al.* (1980) and Duursma (2015).

g_m and C_c were calculated according to Flexas *et al.* (2007), briefly described as follows. The linear electron transport rate (J_t) was estimated as:

$$J_t = \Phi_{PSII} \times \alpha \times 0.5 \times PPFD \quad (1)$$

where α is the fraction of light absorbed by leaves between 0.5 and 0.95, which we estimated by the SPAD value determined by Zheng *et al.* (2021). The partition fraction of photons between PSI and PSII can be assumed as 0.5. Φ_{PSII} was calculated by CF measurements.

The mesophyll conductance (g_m) was calculated as follows:

$$g_m = \frac{P_N}{C_i - \frac{\Gamma^*\left[J_t + 8\left(P_N + R_d\right)\right]}{J_t - 4\left(P_N + R_d\right)}} \quad (2)$$

where P_N, C_i, R_d, and Γ* were calculated from the CO_2-response curve (P_N/C_i) using the *R* package. J_t was calculated by Eq. 1.

The C_c was determined as:

$$C_c = C_i - P_N/g_m \quad (3)$$

The limitation to P_N was following the approach of Jákli *et al.* (2017), which was based on the P_N/C_c curve, briefly described as follows:

$$L_s = \frac{\frac{g_{tot}}{g_s}\cdot\frac{\partial P_N}{\partial C_c}}{g_{tot} + \frac{\partial P_N}{\partial C_c}} \quad (4)$$

$$L_m = \frac{\frac{g_{tot}}{g_m}\cdot\frac{\partial P_N}{\partial C_c}}{g_{tot} + \frac{\partial P_N}{\partial C_c}} \quad (5)$$

$$L_b = \frac{\frac{g_{tot}}{g_b}\cdot\frac{\partial P_N}{\partial C_c}}{g_{tot} + \frac{\partial P_N}{\partial C_c}} \quad (6)$$

where $\partial P_N/\partial C_c$ is the slope of the P_N/C_c curves calculated over a range of 50–100 μmol mol^{-1}. g_{tot} is the total conductance to CO_2 diffusion from the ambient air into chloroplasts:

$$g_{tot} = (1/g_s + 1/g_m)^{-1} \quad (7)$$

The electron fluxes in the photosynthetic carbon reduction cycle [$J_{e(PCR)}$], photorespiratory carbon oxidation cycle [$J_{e(PCO)}$], and alternative electron flux (J_a) were calculated according to Gao *et al.* (2018):

$$J_{e(PCR)} = 4 \times \frac{P_N + R_d}{1 - \frac{\Gamma^*}{C_i}} \quad (8)$$

$$J_{e(PCO)} = 2 \times \Gamma^*/C_i \quad (9)$$

$$J_{e(PCO)} = J_t - J_{e(PCR)} - J_{e(PCO)} \quad (10)$$

where P_N, R_d, C_i, and Γ* were obtained from P_N/C_i curves.

Statistical analysis: The results are reported as the means with standard errors (SE). The significance of the results was checked by *Duncan*'s multiple range tests using *IBM SPSS Statistics 21*.

Results

Gas-exchange parameters and PNUE: Low and moderate N applications (N_{120} and N_{240}) could improve the P_N of both genotypes, but the P_N of *Jimai5265yg* was more sensitive to N applications (Table 1). There was no significant difference in P_N between the mutant and the wild type except for the N_{240} application. However, the PNUE of *Jimai5265yg* was significantly higher than that of the wild type in all N conditions, especially for N_0 and N_{240} (17.1 and 19.9%, respectively). There was no significant difference between genotypes or N applications for $V_{c,max}$ and J_{max}. N (N_{360}) excess increased the Γ* of both genotypes, suggesting that excessive N enhanced photorespiration. PIB has been used to measure the photorespiration rate (Vines *et al.* 1983). The increase of PIB and R_L in both genotypes under N_{240} and N_{360} applications confirmed the increase of photorespiration by high N (Table 2). The Γ* and R_d of *Jimai5265yg* also increased under N_0 application without the increase of PIB (Tables 1, 2). However, the wild type had a significantly higher R_d than that of *Jimai5265yg* in the N_{360} condition (Table 2).

There was a significant nitrogen effect on L_m and L_b for two genotypes (Fig. 1). The difference between the two genotypes was more remarkable in response to low N (N_0 and N_{120}) than to high N (N_{240} and N_{360}) for L_m. The L_m of *Jimai5265yg* was significantly lower than that of the wild type due to higher g_m and C_c under N_0 application (Table 2, Fig. 1). Correspondingly, L_b of *Jimai5265yg* was significantly higher than that of the wild type. In contrast, the L_m of the wild type was larger for low N applications due to reduced g_m and C_c.

Chlorophyll *a* fluorescence parameters: The previous study showed that N_0 and N_{360} induced the decline of SPAD value which indicated the Chl content (Zheng *et al.* 2021). Similarly, the minimal and maximal fluorescence F_0 and F_m significantly decreased in response to N_0 and N_{360} applications (Table 3). The level of F_0 and F_m was significantly lower in *Jimai5265yg* than in its wild type for N_0 and N_{120} application. The lower F_m might be associated with PSII photoinhibition damage. Two genotypes had a lower maximal efficiency of PSII photochemistry (F_v/F_m) in the N_{120} condition. *Jimai5265yg* maintained a slightly higher F_v/F_m than that of the wild type, especially for the N_{240} application (Table 3). There was no significant difference in P_m between different N applications for both genotypes, but the mutant had a slightly lower P_m than the wild type, indicating that the active PSI reaction centers were insensitive to N treatment (Table 3). The quantum yield of PSII (Φ_{PSII}) decreased with the increase of PAR (Fig. 2*A*). Compared to N_{120} and N_{240} applications, N_0 and N_{360} applications induced the increase of Φ_{PSII} and q_P in *Jimai5265yg*, while only the N_{360} application increased Φ_{PSII} and q_P of the wild type. So *Jimai5265yg* has a significantly higher Φ_{PSII} and q_P than the wild type in the N_0 condition (Fig. 2*A*,*D*). In contrast, *Jimai5265yg* has a significantly lower Φ_{NPQ} than that of the wild type in the N_0 condition. Excessive

Table 1. The effects of different N applications on P_N, C_i, Γ*, V_{cmax}, J_{max}, g_m, g_s, C_c, and PNUE in Jimai5265 and *Jimai5265yg* at anthesis. P_N – net photosynthetic rate; C_i – intercellular CO_2 concentration; Γ* – CO_2-compensation point; $V_{c,max}$ – maximum carboxylation rate limited by Rubisco; J_{max} – the light-saturated potential rate of electron transport; g_m – mesophyll conductance; g_s – stomatal conductance; C_c – CO_2 concentration inside the chloroplast; PNUE – photosynthetic N-use efficiency. Results are represented as mean ± standard error, n = 3. Means in a row followed by *different lowercase letters* are significantly different at $p \leq 0.05$ compared *via Duncan*'s multiple range tests. N – different N concentrations; G – genotype. NS – not significant; **$p \leq 0.01$; *$p \leq 0.05$.

	N_0		N_{120}		N_{240}		N_{360}		Analysis of variance		
	Jimai5256	*Jimai5256yg*	Jimai5256	*Jimai5256yg*	Jimai5256	*Jimai5256yg*	Jimai5256	*Jimai5256yg*	N	G	N × G
P_N [μmol(CO_2) m^{-2} s^{-1}]	24.457 ± 1.203^{a}	24.278 ± 1.747^{a}	24.641 ± 0.325^{a}	26.515 ± 1.453^{a}	25.759 ± 0.418^{a}	29.898 ± 0.621^{b}	24.029 ± 0.291^{a}	26.639 ± 0.200^{a}	*	**	NS
C_i [μmol mol^{-1}]	223.973 ± 5.979^{a}	233.949 ± 17.411^{a}	259.904 ± 20.012^{a}	266.039 ± 7.961^{a}	239.928 ± 19.983^{a}	269.247 ± 17.988^{a}	250.709 ± 10.568^{a}	251.362 ± 8.233^{a}	NS	NS	NS
Γ* [μmol mol^{-1}]	45.603 ± 0.484^{a}	64.084 ± 1.517^{c}	46.272 ± 2.013^{a}	47.967 ± 0.796^{ab}	47.967 ± 0.796^{ab}	47.967 ± 0.796^{ab}	60.148 ± 4.699^{c}	53.985 ± 1.464b	**	NS	**
$V_{c,max}$ [μmol(CO_2) m^{-2} s^{-1}]	66.099 ± 5.282^{ab}	50.014 ± 9.618^{a}	77.265 ± 3.737^{ab}	85.594 ± 16.412^{ab}	88.924 ± 12.054^{b}	70.052 ± 1.236^{ab}	63.505 ± 5.992^{ab}	75.081 ± 2.415^{b}	NS	NS	NS
J_{max} [μmol m^{-2} s^{-1}]	169.651 ± 20.044^{abc}	140.059 ± 25.942^{a}	177.153 ± 7.485^{abc}	153.981 ± 20.461^{ab}	210.264 ± 35.136^{bc}	163.849 ± 6.491^{abc}	183.149 ± 8.302^{abc}	221.645 ± 14.961^{c}	NS	NS	NS
g_m [× 10^{-2} mol m^{-2} s^{-1}]	0.227 ± 0.025^{a}	0.461 ± 0.014^{b}	0.255 ± 0.041^{a}	0.291 ± 0.039^{a}	0.276 ± 0.042^{a}	0.313 ± 0.046^{a}	0.274 ± 0.044^{a}	0.285 ± 0.0319^{a}	*	NS	NS
g_s [mol m^{-2} s^{-1}]	0.326 ± 0.003^{a}	0.385 ± 0.029^{a}	0.574 ± 0.214^{a}	0.425 ± 0.048^{a}	0.321 ± 0.071^{a}	0.415 ± 0.143^{a}	0.317 ± 0.037^{a}	0.398 ± 0.003^{a}	NS	NS	NS
C_c [μmol mol^{-1}]	115.081 ± 11.966^{a}	181.210 ± 13.951^{b}	158.764 ± 16.670^{ab}	172.622 ± 4.443^{b}	142.099 ± 9.807^{ab}	169.533 ± 19.742^{b}	158.921 ± 19.911^{ab}	155.801 ± 9.913^{ab}	*	NS	NS
PNUE	3.709 ± 0.469^{ab}	4.476 ± 0.468^{b}	3.694 ± 0.173^{ab}	3.991 ± 0.327^{ab}	3.281 ± 0.245^{a}	4.071 ± 0.239^{ab}	3.418 ± 0.129^{a}	3.51 ± 0.080^{ab}	NS	*	NS

Table 2. The effects of different N applications on PIB, R_L, and R_d in Jimai5265 and *Jimai5265yg* at anthesis. PIB – post-illumination burst; R_L – light respiration rate; R_d – mitochondrial CO_2 release in the dark. Data are expressed as means ± standard error, n = 3. *Lowercase letters* following the data within the same row refer to a significant difference ($p \leq 0.05$), compared *via Duncan*'s multiple range tests. N – nitrogen treatment; G – genotype. NS – not significant; **$p \leq 0.01$; *$p \leq 0.05$.

	N_0		N_{120}		N_{240}		N_{360}		Analysis of variance		
	Jimai5256	*Jimai5256yg*	Jimai5256	*Jimai5256yg*	Jimai5256	*Jimai5256yg*	Jimai5256	*Jimai5256yg*	N	G	N × G
PIB [μmol(CO_2) m^{-2} s^{-1}]	1.820 ± 0.137^{b}	1.390 ± 0.225^{b}	1.876 ± 0.074^{b}	1.916 ± 0.330^{b}	2.859 ± 0.114^{a}	2.605 ± 0.004^{a}	2.983 ± 0.151^{a}	2.710 ± 0.294^{a}	**	NS	NS
R_L [μmol(CO_2) m^{-2} s^{-1}]	1.506 ± 0.047^{c}	1.324 ± 0.026^{c}	1.473 ± 0.049^{c}	1.596 ± 0.095^{c}	2.642 ± 0.018^{a}	2.126 ± 0.176^{b}	2.568 ± 0.225^{a}	2.200 ± 0.071^{b}	**	*	NS
R_d [μmol m^{-2} s^{-1}]	1.700 ± 0.182^{bc}	2.471 ± 0.102^{d}	1.479 ± 0.043^{b}	1.208 ± 0.010^{ab}	0.761 ± 0.022^{a}	1.314 ± 0.133^{ab}	2.340 ± 0.245^{cd}	1.465 ± 0.440^{b}	**	*	**

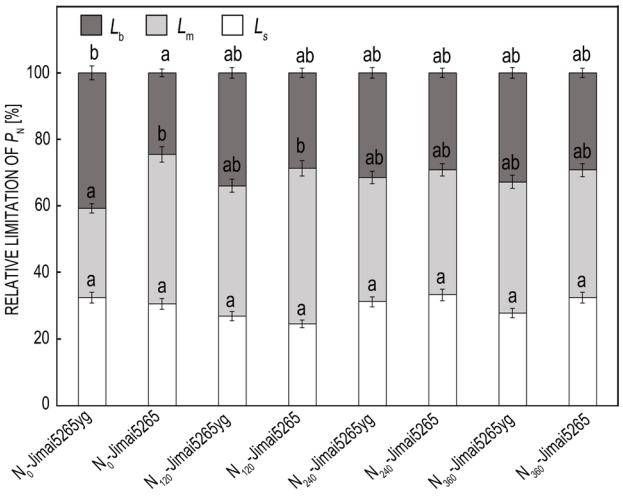

Fig. 1. Relative limitations to photosynthetic rate by L_m, L_s, and L_b in the flag leaves at anthesis. L_b – limitation of biochemical capacity; L_m – limitation of mesophyll diffusion; L_s – limitation of stomatal diffusion. Error bar showed ± standard error from three replicates. The significant difference was calculated using *Duncan*'s multiple range test. *Different letters* indicate significant differences ($p \leq 0.05$) between the respective traits.

N (N_{360}) reduced the Φ_{NPQ} of the wild type. N_{120} and N_{240} have a reverse effect on Φ_{NO} in two genotypes (Fig. 2*B*,*C*). In the N_0 condition, Φ_{NO} of *Jimai5265yg* was significantly higher than that of the wild type, while Φ_{NO} of *Jimai5265yg* was significantly lower in the N_{240} application (Fig. 2*C*).

Φ_{PSI} was significantly higher in *Jimai5265yg* than that of the wild type under N_{120} application when PAR was lower than 500 µmol(photon) m^{-2} s^{-1} (Fig. 2*E*). Φ_{PSI} of *Jimai5265yg* was maintained higher when the PAR increased, except for 329 µmol(photon) m^{-2} s^{-1} in the N_0 and N_{240} conditions. Compared with other three N applications, N_{360} increased Φ_{PSI} of the wild type as the PAR increased. There was no significant difference between *Jimai5265yg* and its wild type in Φ_{ND} with few PAR exceptions (Fig. 2*G*). However, Φ_{NA} of *Jimai5265yg* was significantly lower than that of the wild type under low N applications (N_0 and N_{120}) when PAR was less than 329 µmol(photon) m^{-2} s^{-1} (Fig. 2*F*). Though extreme N applications (N_0 and N_{360}) increased Φ_{NA} in *Jimai5265yg*, the Φ_{NA} of the mutant kept relatively lower than the in the N_0 condition, indicating the decrease of PSI acceptor-side reduction status.

Electron transport rate: The quantum efficiency and photoinhibition process of PSI and PSII was regulated by electron transport. Compared to other N concentrations, N_{360} increased the ETRI and ETRII of the wild type. Besides the N_{360} condition, *Jimai5265yg* had higher ETRI and ETRII in the N_0 condition. As a result, the ETRI and ETRII were significantly higher in *Jimai5265yg* than those in the wild type in the N_0 condition (Fig. 3). Under all N concentrations, the mutant had a significantly higher $J_{e(PCR)}$ (Table 4), indicating the increase of electron

Table 3. The effects of different N applications on P_m, F_0, F_0', F_m, and F_v/F_m in Jimai5265 and *Jimai5265yg* at anthesis. P_m – maximum P700 signal measured using saturation light pulse following short far-red pre-illumination in the dark-adapted state; F_0 – minimum fluorescence; F_0' – minimum fluorescence in the actinic light; F_m – maximum fluorescence; F_v/F_m – maximum quantum efficiency of PSII photochemistry. Values are means ± standard error ($n = 4$). *Lowercase letters* following the data within the same row refer to a significant difference ($p \leq 0.05$), compared *via Duncan*'s multiple range tests. N – nitrogen treatment; G – genotype. NS – not significant; $^{**}p \leq 0.01$; $^{*}p \leq 0.05$.

	N_0		N_{120}		N_{240}		N_{360}		Analysis of variance		
	Jimai5256	*Jimai5256yg*	Jimai5256	*Jimai5256yg*	Jimai5256	*Jimai5256yg*	Jimai5256	*Jimai5256yg*	N	G	N × G
P_m	0.428 ± 0.010^{b}	0.384 ± 0.012^{b}	0.424 ± 0.034^{b}	0.288 ± 0.029^{a}	0.418 ± 0.038^{b}	0.372 ± 0.015^{b}	0.433 ± 0.020^{b}	0.390 ± 0.024^{b}	NS	*	NS
F_0	0.364 ± 0.003^{bc}	0.334 ± 0.004^{a}	0.417 ± 0.012^{e}	0.387 ± 0.010^{cd}	0.399 ± 0.013^{de}	0.374 ± 0.008^{bcd}	0.365 ± 0.003^{bc}	0.351 ± 0.009^{ab}	*	NS	NS
F_0'	0.319 ± 0.002^{ab}	0.313 ± 0.006^{a}	0.353 ± 0.006^{d}	0.344 ± 0.006^{cd}	0.353 ± 0.008^{d}	0.330 ± 0.003^{bc}	0.332 ± 0.003^{bc}	0.318 ± 0.004^{ab}	**	NS	NS
F_m	2.054 ± 0.011^{b}	1.913 ± 0.020^{a}	2.197 ± 0.026^{c}	2.049 ± 0.030^{b}	2.202 ± 0.031^{c}	2.165 ± 0.027^{c}	2.028 ± 0.021^{b}	2.029 ± 0.028^{b}	*	NS	*
F_v/F_m	0.823 ± 0.001^{b}	0.827 ± 0.001^{b}	0.812 ± 0.003^{a}	0.812 ± 0.004^{a}	0.812 ± 0.005^{a}	0.828 ± 0.002^{b}	0.819 ± 0.001^{ab}	0.828 ± 0.002^{b}	**	**	NS

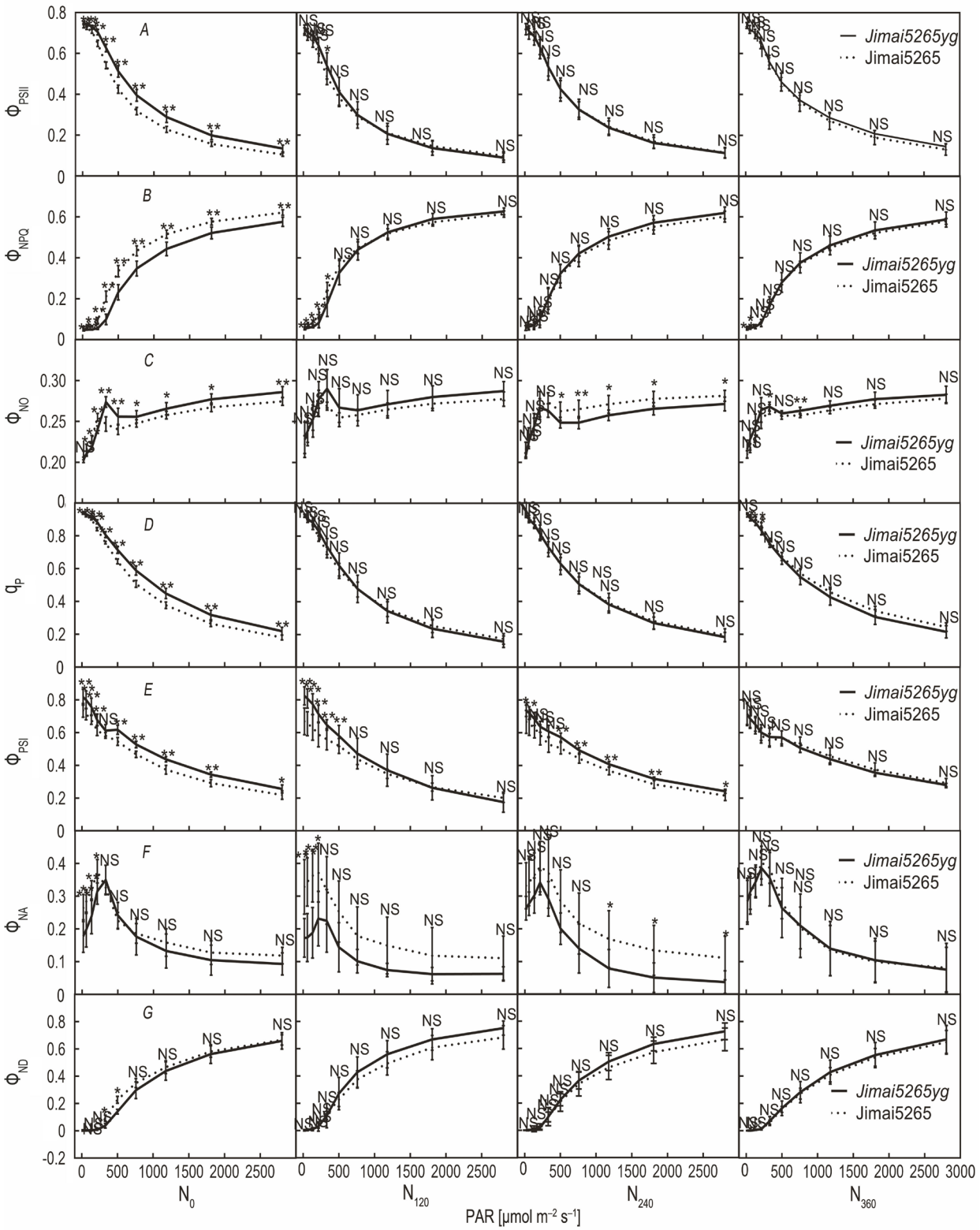

Fig. 2. The light-response curves of parameters derived from chlorophyll fluorescence in flag leaves of Jimai5265 and *Jimai5265yg* at anthesis under four N concentrations. Φ_{PSII} – effective quantum yield of PSII (*A*); Φ_{NPQ} – quantum yield of nonphotochemical quenching (*B*); Φ_{NO} – quantum yield of nonregulated energy loss in PSII (*C*); q_P – photochemical quenching (*D*); Φ_{PSI} – effective quantum yield of PSI (*E*); Φ_{NA} – redox poise of PSI acceptor site (*F*); Φ_{ND} – redox poise of PSI donor site (*G*). The significant difference was calculated using *Duncan*'s multiple range test. *The asterisk* showed differences between the two genotypes within the same N concentration. NS – not significant; $^{**}p \leq 0.01$; $^{*}p \leq 0.05$.

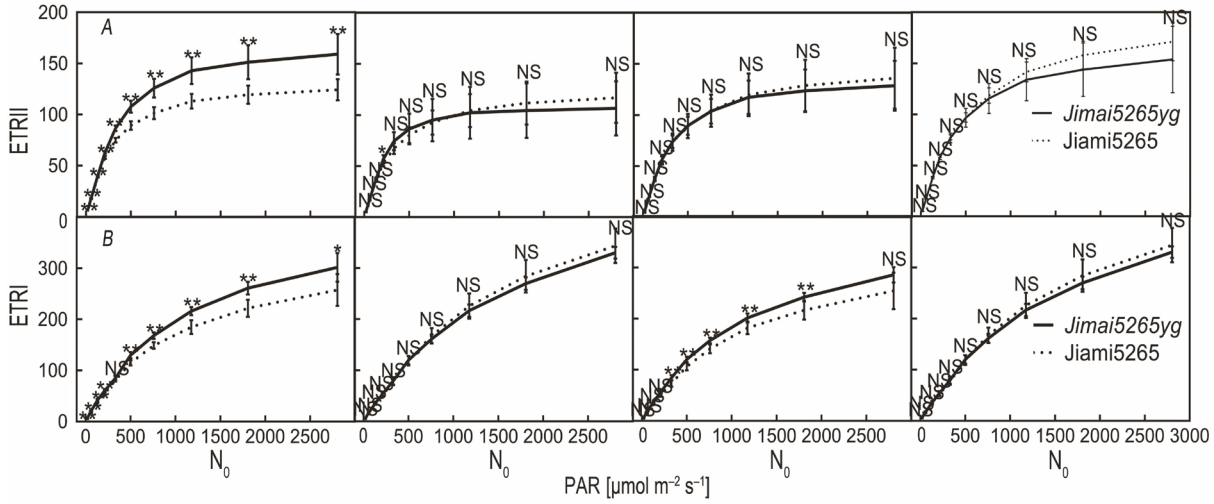

Fig. 3. The light-response curves of ETRII and ETRI in flag leaves of Jimai5265 and *Jimai5265yg* at anthesis under four N concentrations. ETRII – electron transport rate of PSII (*A*); ETRI – electron transport rate of PSI (*B*). The results were shown as mean value ± SD. The significant difference was calculated using *Duncan*'s multiple range test. *The asterisk* showed differences between the two genotypes within the same N concentration. NS – not significant; $^{**}p \leq 0.01$; $^{*}p \leq 0.05$.

flux to the CO_2 assimilation. There was no significant difference between N_{120}, N_{240}, and N_{360} applications on the J_t, $J_{e(PCO)}$, and J_a of the two genotypes (Table 4). However, *Jimai5265yg* had significantly lower J_t, $J_{e(PCO)}$, and J_a than the wild type in the N_0 condition, indicating that the electron transport of *Jimai5265yg* was downregulated.

Principal component analyses: To determine the best set of dependent variables associated with each genotype and with the N applications, PCA was performed based on the original values of all variables. The first and the second components (PC1 and PC2) explained 40% and 25.5% variation, respectively (Fig. 4). Two genotypes were not separated by PCA, but *Jimai5265yg* separately followed a positive direction with P_N, g_m, ETRI, Φ_{PSI}, g_s, Φ_{NO}, C_c, and $J_{e(PCR)}$. Other variables were positively related to both genotypes (Fig. 4*A*,*C*). N_{120} separated from N_0, N_{240}, and N_{360} and followed a positive direction with C_i, Φ_{ND}, Φ_{NPQ} N_{area}, F_0, $V_{c,max}$, which were negatively correlated with the load score of PC1. N_0 and N_{360} applications exhibited positive values in PC2 and PC1, respectively, and followed a positive direction with F_v/F_m, $J_{e(PCO)}$, q_P, ETRII, Γ^*, Φ_{PSII}. The grain yield per spike was more closely related to J_a, P_m, J_t, Φ_{NA}, and PNUE.

Discussion

The parameters of gas exchange, chlorophyll fluorescence, and electron transport in two genotypes were studied under four N concentrations in the field. The findings presented here proved that photoprotection was crucial for crop productivity and could serve as a new breeding strategy. Although N deficiency decreased the P_N in the field experiment, the reduction was less dramatic than in our previous hydroponic experiment. It has been reported that the rate of photosynthesis per unit leaf area changed little during intensive breeding for most crops due to the inexpensive N fertilizer, which reduced the selection pressure for photosynthesis improvement (Jahn *et al.* 2011). The photosynthetic capacity of modern crops was sufficient to increase grain yield (Richards 2000). At anthesis, low or high N conditions might affect the net carbon gain per unit ground area rather than per unit leaf area due to the change of total leaf area. The total leaf area, leaf area duration, and N content were more critical for the grain yield. For early growth, photosynthesis was the determinant for leaf growth rather than the leaf area since the leaf had not been fully expanded (Liu *et al.* 2018). The photosynthetic rate was more likely to be influenced by N treatments during the seedling stage (Li *et al.* 2021). However, we observed a few differences in P_N between N treatments for both genotypes at anthesis (Table 1). Similar to the previous study, P_N of the late growth stage was less sensitive to N applications (Richards 2000). P_N of *Jimai5265yg* was significantly higher than that of the wild type under N_{240} applications (Table 1), suggesting that the photosynthetic advantages of *Jimai5265yg* were dependent on the N application. However, PCA analysis revealed that the grain yield under N_0 was not necessarily connected to the net photosynthetic rate (Fig. 4). According to the study by Richards (2000), the photosynthetic rate of the whole crop population was more closely related to the grain yield.

It has been found that some photosynthetic processes, such as stomatal conductance (g_s) and maximum photosynthetic rate, were associated with grain yield formation (Fischer *et al.* 1998). We estimated the limitations (L_s, L_m, L_b) to photosynthesis under different N applications in quantification. Three limitations exhibited no significant difference under high N conditions (N_{240} and N_{360}), but L_b and L_m increased for *Jimai5265yg* and the wild type respectively under low N conditions (N_0 and N_{120}) (Fig. 1).

Table 4. The effects of different N applications on J_t, $J_{e(PCR)}$, $J_{e(PCO)}$, and J_a in Jimai5265 and *Jimai5265yg* at anthesis. J_t – electron transport rate; $J_{a(PCR)}$ – electron flux to photosynthetic carbon reduction; $J_{a(PCO)}$ – electron flux to photorespiratory carbon oxidation; J_a – alternative electron flux. Values are means ± standard error, n = 3. *Lowercase letters* following the data within the same row refer to a significant difference ($p \leq 0.05$), compared *via Duncan*'s multiple range tests. N – nitrogen treatment; G – genotype. NS – not significant; $^{**}p \leq 0.01$; $^{*}p \leq 0.05$.

	N_0		N_{120}		N_{240}		N_{360}		Analysis of variance		
	Jimai5256	*Jimai5256yg*	Jimai5256	*Jimai5256yg*	Jimai5256	*Jimai5256yg*	Jimai5256	*Jimai5256yg*	N	G	N × G
J_t [μmol^{-1} m^{-2}s^{-1}]	337.427 ± 2.824^{d}	265.094 ± 6.374^{b}	221.161 ± 10.973^{a}	234.845 ± 2.979^{a}	286.248 ± 1.585^{c}	295.249 ± 3.439^{e}	283.423 ± 3.380^{e}	285.047 ± 2.337^{c}	**	*	**
$J_{e(PCR)}$ [μmol^{-1} m^{-2}s^{-1}]	140.209 ± 1.016^{b}	169.448 ± 4.161^{f}	126.289 ± 1.306^{a}	161.015 ± 2.743^{ef}	146.957 ± 1.939^{bcd}	149.511 ± 4.119^{cd}	143.925 ± 2.468^{bc}	154.876 ± 1.010^{de}	*	**	**
$J_{e(PCO)}$ [μmol^{-1} m^{-2}s^{-1}]	0.425 ± 0.007^{a}	0.607 ± 0.013^{d}	0.418 ± 0.017^{a}	0.446 ± 0.023^{a}	0.581 ± 0.006^{cd}	0.592 ± 0.0139^{d}	0.535 ± 0.010^{bc}	0.506 ± 0.022^{b}	**	**	**
J_a [μmol^{-1} m^{-2}s^{-1}]	162.404 ± 11.957^{c}	85.480 ± 0.991^{a}	88.301 ± 3.496^{a}	82.168 ± 3.038^{a}	143.683 ± 5.333^{b}	145.279 ± 0.560^{bc}	138.963 ± 5.858^{b}	129.665 ± 3.325^{b}	**	**	**

The suboptimal conditions often induced the increase of mesophyll limitation (Brestic *et al.* 2018). The alteration of limitations to P_N might be mediated by the change of mesophyll conductance (g_m) since the difference in $V_{c,max}$ and J_{max} between the two genotypes was not significant (Table 1). Mesophyll conductance was affected by leaf thickness and anatomical structures related to LMA. Low N supply induced the accumulation of nonstructural chemical components and resulted in a higher LMA (Pan *et al.* 2011). However, *Jimai5265yg* has significantly higher g_m than the wild type without the diversity in LMA in the N_0 condition (Table 2S, *supplement*), indicating that g_m was influenced by other factors rather than LMA, such as the distribution or orientation of chloroplasts and other organelles (Xiong *et al.* 2016). Even if g_m was high, the photosynthesis of *Jimai5265yg* was restricted by carboxylation efficiency in the N_0 condition.

There is no remarkable superiority in net photosynthetic rate for *Jimai5265yg* in the N_0 condition, but *Jimai5265yg* had a significantly higher PNUE. Leaf N concentration is often positively correlated with leaf respiration (Reich *et al.* 2008). The interaction between the photorespiratory pathway and N metabolism determined the leaf N status and the content of photosynthetic proteins (Wingler *et al.* 2000). Photorespiratory ammonia recycling was also dependent on mitochondria function and the products of chloroplasts (Champigny 1995). *Jimai5265yg* has a higher Γ* and R_d in the N_0 condition (Tables 1, 2). The rise of the CO_2-compensation point indicated the increase in photorespiratory CO_2 loss (Colman 1984). The increase of photorespiration in the rice *ygl53* mutant helped balance the high C/N ratio induced by the high photosynthetic efficiency (Liang *et al.* 2021). We proposed that the higher PNUE of *Jimai5265yg* might be associated with higher photorespiration, which influenced the leaf N status and facilitated the internal nitrogen remobilization. Leaf N status and remobilization positively correlated with spike differentiation, pollen fertility, and the subsequent grain yield (Reynolds *et al.* 2012). PCA showed that the grain yield was closely related to PNUE rather than P_N. The greater grain number per spike for *Jimai5265yg* in the N_0 condition observed by Zheng *et al.* (2021) might result from improved N reassimilation and remobilization efficiency.

Besides participating in the carbon and nitrogen cycles, the photorespiratory pathway was essential for protecting PSII from photoinhibition by consuming the excess photochemical energy and repairing the photodamaged PSII (Takahashi *et al.* 2007). F_0 had been used as the indicator for irreversible damage of PSII as the temperature increased. The rise of F_0 was related to the disconnection of LHCII from the core PSII center and the reduction of PSII (Pastenes and Horton 1999). The lower F_0 provided the basal protection of PSII in *Jimai5265yg* in the field where intense light and high temperature were inevitable (Table 3). The reduction of F_v/F_m reflected the photoinhibition and damage of PSII complexes. N-deficiency caused a decrease in F_v/F_m in many species, such as tea, *Panax notoginseng*, maize,

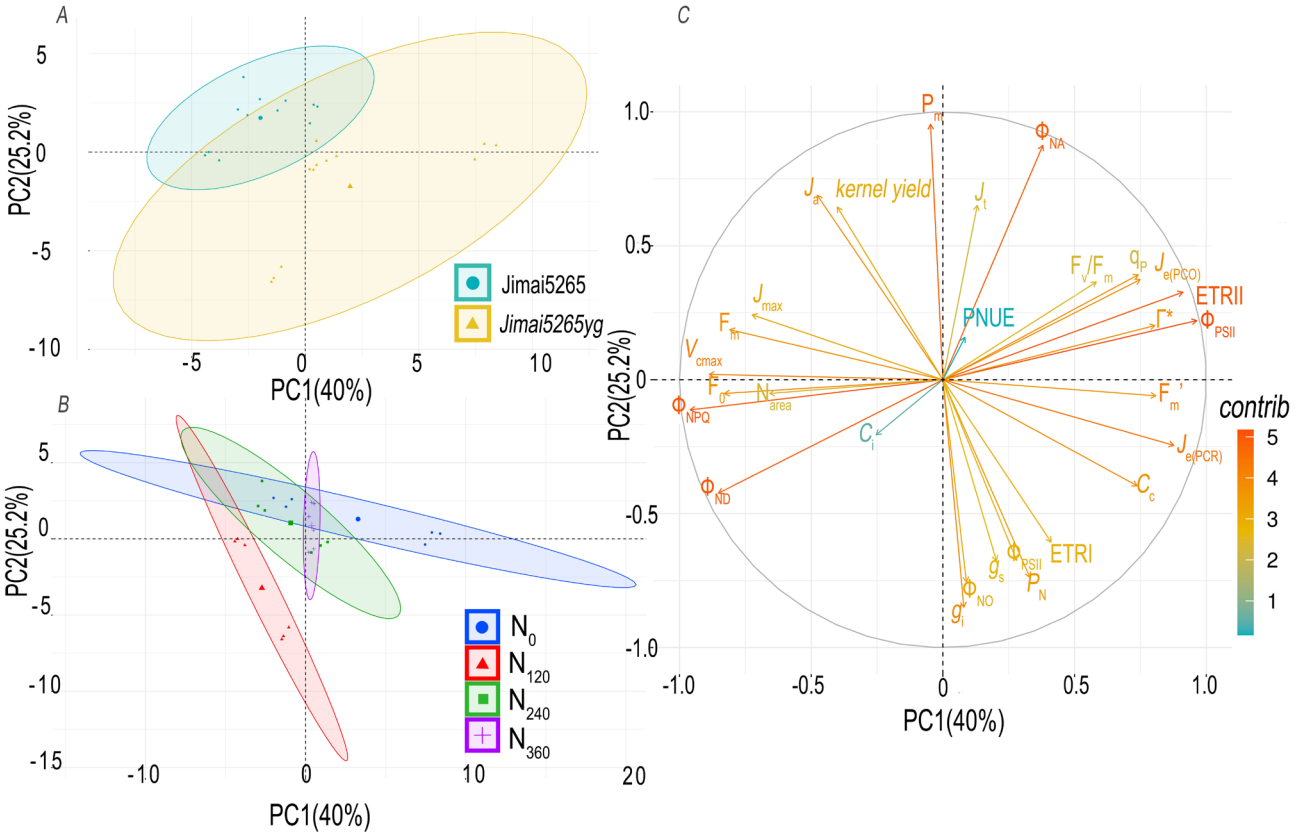

Fig. 4. Principal component analysis of gas-exchange parameters, chlorophyll fluorescence parameters, PNUE, leaf N content, and grain yield of two genotypes under four N concentrations at anthesis. Individual representation of wheat genotypes (*A*); N concentrations for each genotype (*B*); genotypes and N concentrations associated with variables studied on principal component analysis (*C*). C_c – CO_2 concentration inside the chloroplast; C_i – intercellular CO_2 concentration; ETRI – electron transport rate of PSI; ETRII – electron transport rate of PSII; F_0 – minimum fluorescence; F_m – maximum fluorescence; F_m' – maximum fluorescence in the actinic light; F_v/F_m – maximum quantum efficiency of PSII photochemistry; g_s – stomatal conductance; $J_{e(PCO)}$ – electron flux to photorespiratory carbon oxidation; $J_{e(PCR)}$ – electron flux to photosynthetic carbon reduction; J_{max} – light-saturated potential rate of electron transport; J_t – electron transport rate; N_{area} – nitrogen content per unit area; P_m or P_m' – maximum P700 signal measured using saturation light pulse following short far-red pre-illumination in dark- or light-adapted state; P_N – net photosynthetic rate; PNUE – photosynthetic N-use efficiency; q_P – PSII efficiency factor (the fraction of open centers); $V_{c,max}$ – maximum carboxylation rate limited by Rubisco; Γ* – CO_2-compensation point; Φ_{NA} – oxidation status of PSI acceptor site; Φ_{ND} – oxidation status of PSI donor site; Φ_{NO} – quantum yield nonregulated heat dissipation; Φ_{NPQ} – quantum yield of nonphotochemical quenching; Φ_{PSI} – quantum yield of PSI photochemistry; Φ_{PSII} – PSII operating efficiency (quantum yield of PSII photochemistry).

A. thaliana, and rice (Lin *et al.* 2016, Honoki *et al.* 2018, Zhang *et al.* 2020). Though a study of wheat indicated that F_v/F_m parameter was insensitive to N treatment, Gao *et al.* (2018) and our previous study showed a decrease in F_v/F_m for wheat seedlings when N was deficient (Li *et al.* 2021). In this study, F_v/F_m was lower in the N_{120} condition for two genotypes at anthesis (Table 3). F_v/F_m of *Jimai5265yg* was significantly higher than the wild type in the N_{240} condition, suggesting more activated PSII reaction centers and less susceptibility to photoinhibition. High irradiance increased susceptibility to photoinhibition of N-deficient plants, so we observed the light-response curve of q_P (Fig. 2*D*), representing a proportion of the open PSII reaction centers (Lu and Zhang 2000). Many studies proved that low N decreased q_P in maize, bean, and wheat (Antal *et al.* 2010, Jin *et al.* 2015, Kartseva *et al.* 2021). We observed similar results in the wild type for N_0, N_{120}, and N_{240} applications, but N deficiency (N_0) increased q_P of *Jimai5265yg* (Fig. 2*D*), suggesting that low N and extreme N deficiency had different effects on the mutant. It has been reported that the higher reduction level of the primary electron acceptor Q_A increased susceptibility to photoinhibition of PSII (Lu and Zhang 2000). The higher q_P value of *Jimai5265yg* compared to the wild type under N_0 application indicated a lower reduction state of Q_A and lower excitation pressure of the PSII acceptor side. Though there was less excitation energy transferred into the reaction centers, the PSII complex of *Jimai5265yg* was more damaged by photoinhibition in the N_0 condition (lower Φ_{NPQ}). We observed stable P_m in response to different N treatments, suggesting that photochemically active PSI were unaffected. The photo-

inhibition of PSII was an effective protective mechanism for the PSI (Brestic *et al.* 2016).

Nonphotochemical quenching (NPQ) reflecting a thermal dissipation of excess light energy served as a protection of PSII against photoinhibition (Shimakawa and Miyake 2019). The lower Φ_{NPQ} of *Jimai5265yg* in the N_0 condition might contribute to the higher photoinhibition of PSII. However, the quantum yield of the PSII photochemical process (Φ_{PSII}) in *Jimai5265yg* was significantly higher than the wild type in the N_0 condition (Fig. 2*A*). Insufficient or excess N supplies reduced the distribution of light energy to the active PSII reaction center (Φ_{PSII}) and increased energy flow to the nonphotochemical process (NPQ) (Jauffrais *et al.* 2016, Zhang *et al.* 2020). N-deficient wheat and maize showed a reduction in Φ_{PSII}, especially for the low N-sensitive cultivars (Lu and Zhang 2000, Gao *et al.* 2018). Excessive N decreased both Φ_{PSII} and Φ_{NPQ} in *Panax notoginseng* (Cun *et al.* 2021). The PSII photochemical conversion efficiency depended on the excitation energy distribution in PSII complexes. It seems that more proportion of excitation energy was consumed by PSII photochemistry and lost through the nonregulated dissipative pathway (higher Φ_{NO}) for *Jimai5265yg* in the N_0 condition. The higher PSII photochemical efficiency was a benefit for CO_2 assimilation, but the increase of NO was associated with a harmful longer lifetime of energy excitation (Laisk *et al.* 1997). Nonregulated energy dissipation comprised the thermal dissipation in nonfunctional PSIIs and constitutive light-independent thermal dissipation processes (Stirbet and Govindjee 2011). Higher q_P of *Jimai5265yg* induced by N_0 indicated less inactive PSIIs, so the increase of Φ_{NO} was associated with the constitutive light-independent thermal dissipation process (Fig. 2*C*,*D*). The previous study interpreted the higher Φ_{NO} as a more reduced PSII acceptor side or a larger proportion of closed PSII reaction centers; as a result, triplet Chl^* and ROS formed and led to PSII photoinhibition (Samson *et al.* 2019). However, it seems the increase of NO was not dependent on the closure of PSII reaction centers in our experiments (q_P) considering the complementarity of Φ_{PSII}, Φ_{NO}, and Φ_{NPQ} (Fig. 2*A–D*). Although the photochemical efficiency of PSII in *Jimai5265yg* improved under N_0 application, the capacity of PSII photoprotection decreased due to an increase of Φ_{NO} at the expense of the harmless energy dissipation pathway NPQ.

The generation of NPQ was dependent on a transthylakoid proton gradient built up by linear and cyclic electron transport (CET) (Zivcak *et al.* 2014a). Our previous study showed that *Jimai5265yg* had higher CET than the wild type under the N-deficient condition at the seedling stage. The nonphotochemical energy dissipation was enhanced in *Jimai5265yg* due to the increase of oxidized P700 (Φ_{ND}) (Li *et al.* 2021). The increase in the CET rate provided efficient protection against oxidative stress, such as heat, high light, and drought (Zivcak *et al.* 2014a,b). We did not observe a significant difference in CET (Φ_{PSI}/Φ_{PSII}) between the two genotypes, but the higher Φ_{PSI} of *Jimai5265yg* under N_0, N_{120}, and N_{240} indicated that the photochemical efficiency of PSI increased (Fig. 2*E*). The photochemical reaction in PSI was limited by the oxidation status of the donor side (Φ_{ND}) and the reduction status of the acceptor side (Φ_{NA}). It has been documented that N deficiency induced the over-reduction of the PSI acceptor side and led to PSI photoinhibition. A wheat *chlorina* mutant *ANK* has a more reduced acceptor side of PSI and inactive PSI despite normal NPQ level (Brestic *et al.* 2016). In contrast, the PSI acceptor side of *Jimai5265yg* (Φ_{NA}) was less reduced than that of the wild type at low light conditions with insufficient N applications (N_0 and N_{120}) (Fig. 2*F*), indicating that PSI was photoinhibited less. It has been assumed that downregulated electron transport protected the acceptor side of PSI against over-reduction. The photodamaged PSII prevented electron transfer to PSI and, therefore, further production of ROS (Tikkanen and Aro 2014). According to our results, the PSII of *Jimai5265yg* was more susceptible to photodamage because of its lower capacity to trigger NPQ. Meanwhile, the PSII protected PSI against oxidative damage by adjusting electron flow.

Studies using wheat seedlings revealed that low or deficient N conditions reduced the electron transport rate due to the decreased carboxylation rate (Gao *et al.* 2018, Li *et al.* 2021). Consistently, we observed that J_t of *Jimai5265yg* was significantly lower in low and deficient N (N_0 and N_{120}) compared to N_{240} and N_{360} conditions (Table 4). However, the wild type had a higher J_t under the N_0 condition. As a result, the difference between the two genotypes on electron transport rate was more significant for the N_0 condition. Despite lower J_t, *Jimai5265yg* had a higher $J_{e(PCR)}$, suggesting more electrons flow to the carboxylation process. The electron flow through PSII (ETRII), which was required by carboxylation and oxygenation, was also higher in the N_0 condition for *Jimai5265yg* (Fig. 3*A*). Photorespiratory or Mehler pathway could serve as another energy sink for dissipation of excess excitation energy under stress conditions (Wingler *et al.* 2000, Huang *et al.* 2019). The higher $J_{e(PCO)}$ and Γ^* indicated that photorespiration was essential for the excessive energy consumption of *Jimai5265yg* (Tables 1, 4). However, J_a is important for the wild type to prevent photoinhibition when J_t was higher in the N_0 condition. To eliminate excessive electrons, *Jimai5265yg* was dependent on reducing electron transport rate and photorespiration, while NPQ and other processes such as the Mehler pathway were more critical for its wild type to cope with N deficiency.

Conclusion and future perspective: Our results demonstrated that different N applications had little effect on the net photosynthetic rate at anthesis for two genotypes. The yellow-green mutant *Jimai5265yg* had a higher PNUE, which might be associated with N metabolism regulated by the photorespiratory pathway. Despite the lower NPQ, *Jimai5265yg* had higher photochemical efficiency of PSI and PSII and lower reduction status of the PSI acceptor side. The photodamaged PSII protected PSI from over-reduction by regulating electronic transport. Besides, the increased photorespiration was the electron

sink for energy dissipation. Though the P_N advantage of the mutant was not clear at anthesis, the protective capability against photodamage of PSI was enhanced under the N-deficient condition (N_0). It seems that photoprotection and its related electron transport of PSII and PSI might be associated with the productivity of the mutant in the N-deficient field. Our results may open new possibilities for improving grain yield or spike development of N-deficient wheat by manipulating the photoprotective mechanism. Photoprotection was dependent on the light-harvesting machinery composition and structure, thylakoid components, and the xanthophyll cycle, which has not been studied in *Jimai5265yg*. Further investigation on N absorption, metabolism, and remobilization in *Jimai5265yg* may help explain why the mutant has a higher grain yield in the N-deficient field.

References

Antal T., Mattila H., Hakala-Yatkin M. *et al.*: Acclimation of photosynthesis to nitrogen deficiency in *Phaseolus vulgaris*. – Planta **232**: 887-898, 2010.

Ayub G., Smith R.A., Tissue D.T. *et al.*: Impacts of drought on leaf respiration in darkness and light in *Eucalyptus saligna* exposed to industrial-age atmospheric CO_2 and growth temperature. – New Phytol. **190**: 1003-1018, 2011.

Benedict C.R., McCree K.J., Kohel R.J.: High photosynthetic rate of a chlorophyll mutant of cotton. – Plant Physiol. **49**: 968-971, 1972.

Bielczynski L.W., Schansker G., Croce R.: Consequences of the reduction of the Photosystem II antenna size on the light acclimation capacity of *Arabidopsis thaliana*. – Plant Cell Environ. **43**: 866-879, 2020.

Brestic M., Zivcak M., Hauptvogel P. *et al.*: Wheat plant selection for high yields entailed improvement of leaf anatomical and biochemical traits including tolerance to non-optimal temperature conditions. – Photosynth. Res. **136**: 245-255, 2018.

Brestic M., Zivcak M., Kunderlikova K., Allakhverdiev S.I.: High temperature specifically affects the photoprotective responses of chlorophyll *b*-deficient wheat mutant lines. – Photosynth. Res. **130**: 251-266, 2016.

Byeon S., Song W., Park M. *et al.*: Down-regulation of photosynthesis and its relationship with changes in leaf N allocation and N availability after long-term exposure to elevated CO_2 concentration. – J. Plant Physiol. **265**: 153489, 2021.

Champigny M.L.: Integration of photosynthetic carbon and nitrogen metabolism in higher plants. – Photosynth. Res. **46**: 117-127, 1995.

Colman B.: The effect of temperature and oxygen on the CO_2 compensation point of the marine alga *Ulva lactuca*. – Plant Cell Environ. **7**: 619-621, 1984.

Cun Z., Zhang J.-Y., Wu H.-M. *et al.*: High nitrogen inhibits photosynthetic performance in a shade-tolerant and N-sensitive species *Panax notoginseng*. – Photosynth. Res. **147**: 283-300, 2021.

Duursma R.A.: Plantecophys – An R package for analysing and modelling leaf gas exchange data. – PLoS ONE **10**: e0143346, 2015.

Farquhar G.D., von Caemmerer S., Berry J.A.: A biochemical model of photosynthetic CO_2 assimilation in leaves of C_3 species. – Planta **149**: 78-90, 1980.

Fischer R.A., Rees D., Sayre K.D. *et al.*: Wheat yield progress associated with higher stomatal conductance and photosynthetic rate, and cooler canopies. – Crop Sci. **38**: 1467-1475, 1998.

Flexas J., Ortuño M.F., Ribas-Carbo M. *et al.*: Mesophyll conductance to CO_2 in *Arabidopsis thaliana*. – New Phytol. **175**: 501-511, 2007.

Gao J., Wang F., Sun J. *et al.*: Enhanced Rubisco activation associated with maintenance of electron transport alleviates inhibition of photosynthesis under low nitrogen conditions in winter wheat seedlings. – J. Exp. Bot. **69**: 5477-5488, 2018.

Genesio L., Bassi R., Miglietta F.: Plants with less chlorophyll: a global change perspective. – Glob. Change Biol. **27**: 959-967, 2021.

Gu J.F., Zhou Z.X., Li Z.K. *et al.*: Rice (*Oryza sativa* L.) with reduced chlorophyll content exhibit higher photosynthetic rate and efficiency, improved canopy light distribution, and greater yields than normally pigmented plants. – Field Crop. Res. **200**: 58-70, 2017.

Honoki R., Ono S., Oikawa A. *et al.*: Significance of accumulation of the alarmone (p)ppGpp in chloroplasts for controlling photosynthesis and metabolite balance during nitrogen starvation in *Arabidopsis*. – Photosynth. Res **135**: 299-308, 2018.

Hou W.F., Tränkner M., Lu J.W. *et al.*: Interactive effects of nitrogen and potassium on photosynthesis and photosynthetic nitrogen allocation of rice leaves. – BMC Plant Biol. **19**: 302, 2019.

Huang W., Yang Y.J., Wang J.H., Hu H.: Photorespiration is the major alternative electron sink under high light in alpine evergreen sclerophyllous *Rhododendron* species. – Plant Sci. **289**: 110275, 2019.

Jahn C.E., Mckay J.K., Mauleon R. *et al.*: Genetic variation in biomass traits among 20 diverse rice varieties. – Plant Physiol. **155**: 157-168, 2011.

Jákli B., Tavakol E., Tränkner M. *et al.*: Quantitative limitations to photosynthesis in K deficient sunflower and their implications on water-use efficiency. – J. Plant Physiol. **209**: 20-30, 2017.

Jauffrais T., Jesus B., Méléder V. *et al.*: Physiological and photophysiological responses of the benthic diatom *Entomoneis paludosa* (Bacillariophyceae) to dissolved inorganic and organic nitrogen in culture. – Mar. Biol. **163**: 115, 2016.

Jin H., Li M., Duan S. *et al.*: Optimization of light-harvesting pigment improves photosynthetic efficiency. – Plant Physiol. **172**: 1720-1731, 2016.

Jin X., Yang G., Tan C., Zhao C.: Effects of nitrogen stress on the photosynthetic CO_2 assimilation, chlorophyll fluorescence, and sugar-nitrogen ratio in corn. – Sci. Rep.-UK **5**: 9311, 2015.

Kartseva T., Dobrikova A., Kocheva K. *et al.*: Optimal nitrogen supply ameliorates the performance of wheat seedlings under osmotic stress in genotype-specific manner. – Plants-Basel **10**: 493, 2021.

Kramer D.M., Johnson G., Kiirats O., Edwards G.E.: New fluorescence parameters for the determination of Q_A redox state and excitation energy fluxes. – Photosynth. Res. **79**: 209-218, 2004.

Kromdijk J., Głowacka K., Leonelli L. *et al.*: Improving photosynthesis and crop productivity by accelerating recovery from photoprotection. – Science **354**: 857-861, 2016.

Kumari S., Sharma N., Raghuram N.: Meta-analysis of yield-related and N-responsive genes reveals chromosomal hotspots, key processes and candidate genes for nitrogen-use efficiency in rice. – Front Plant Sci. **12**: 627955, 2021.

Laisk A., Oja V., Rasulov B. *et al.*: Quantum yields and rate constants of photochemical and nonphotochemical excitation

quenching (experiment and model). – Plant Physiol. **115**: 803-815, 1997.
Li H.X., Li J.J., Zhang X.H. *et al.*: Mesophyll conductance, photoprotective process and optimal N partitioning are essential to the maintenance of photosynthesis at N deficient condition in a wheat yellow-green mutant (*Triticum aestivum* L.). – J. Plant Physiol. **263**: 153469, 2021.
Li Y., Ren B., Gao L. *et al.*: Less chlorophyll does not necessarily restrain light capture ability and photosynthesis in a chlorophyll-deficient rice mutant. – J. Agron. Crop Sci. **199**: 49-56, 2013.
Liang Y., Wang J., Zeng F. *et al.*: Photorespiration regulates carbon–nitrogen metabolism by magnesium chelatase D subunit in rice. – J. Agr. Food Chem. **69**: 112-125, 2021.
Lin Z.H., Zhong Q.S., Chen C.S. *et al.*: Carbon dioxide assimilation and photosynthetic electron transport of tea leaves under nitrogen deficiency. – Bot. Stud. **57**: 37, 2016.
Liu T., Ren T., White P.J. *et al.*: Storage nitrogen co-ordinates leaf expansion and photosynthetic capacity in winter oilseed rape. – J. Exp. Bot. **69**: 2995-3007, 2018.
Lu C.M., Zhang J.H.: Photosynthetic CO_2 assimilation, chlorophyll fluorescence and photoinhibition as affected by nitrogen deficiency in maize plants. – Plant Sci. **151**: 135-143, 2000.
Nunes-Nesi A., Nascimento V.L., de Oliveira Silva F.M. *et al.*: Natural genetic variation for morphological and molecular determinants of plant growth and yield. – J. Exp. Bot. **67**: 2989-3001, 2016.
Ort D.R., Merchant S.S., Alric J. *et al.*: Redesigning photosynthesis to sustainably meet global food and bioenergy demand. – P. Natl. Acad. Sci. USA **112**: 8529-8536, 2015.
Ort D.R., Zhu X., Melis A.: Optimizing antenna size to maximize photosynthetic efficiency. – Plant Physiol. **155**: 79-85, 2011.
Oxborough K., Baker N.R.: Resolving chlorophyll alpha fluorescence images of photosynthetic efficiency into photochemical and non-photochemical components: calculation of q_P and F_v'/F_m' without measuring F_0'. – Photosynth. Res. **54**: 135-142, 1997.
Pan J.F., Cui K.H., Wei D. *et al.*: Relationships of non-structural carbohydrates accumulation and translocation with yield formation in rice recombinant inbred lines under two nitrogen levels. – Physiol. Plantarum **141**: 321-331, 2011.
Pastenes C., Horton P.: Resistance of photosynthesis to high temperature in two bean varieties (*Phaseolus vulgaris* L.). – Photosynth. Res. **62**: 197-203, 1999.
Reich P.B., Tjoelker M.G., Pregitzer K.S. *et al.*: Scaling of respiration to nitrogen in leaves, stems and roots of higher land plants. – Ecol. Lett. **11**: 793-801, 2008.
Reynolds M., Foulkes J., Furbank R. *et al.*: Achieving yield gains in wheat. – Plant Cell Environ. **35**: 1799-1823, 2012.
Richards R.A.: Selectable traits to increase crop photosynthesis and yield of grain crops. – J. Exp. Bot. **51**: 447-458, 2000.
Rotundo J.L., Cipriotti P.A.: Biological limits on nitrogen use for plant photosynthesis: a quantitative revision comparing cultivated and wild species. – New Phytol. **214**: 120-131, 2017.
Sakowska K., Alberti G., Genesio L. *et al.*: Leaf and canopy photosynthesis of a chlorophyll deficient soybean mutant. – Plant Cell Environ. **41**: 1427-1437, 2018.
Samson G., Bonin L., Maire V.: Dynamics of regulated Y_{NPQ} and non-regulated Y_{NO} energy dissipation in sunflower leaves exposed to sinusoidal lights. – Photosynth. Res. **141**: 315-330, 2019.
Shimakawa G., Miyake C.: What quantity of photosystem I is optimum for safe photosynthesis? – Plant Physiol. **179**: 1479-1485, 2019.
Slattery R.A., Ort D.R.: Perspectives on improving light distribution and light use efficiency in crop canopies. – Plant Physiol. **185**: 34-48, 2021.
Stirbet A., Govindjee: On the relation between the Kautsky effect (chlorophyll *a* fluorescence induction) and Photosystem II: Basics and applications of the OJIP fluorescence transient. – J. Photoch. Photobio. B **104**: 236-257, 2011.
Takahashi S., Bauwe H., Badger M.: Impairment of the photorespiratory pathway accelerates photoinhibition of photosystem II by suppression of repair but not acceleration of damage processes in *Arabidopsis*. – Plant Physiol. **144**: 487-494, 2007.
Terao T., Katoh S.: Antenna sizes of photosystem I and photosystem II in chlorophyll *b*-deficient mutants of rice. Evidence for an antenna function of photosystem II centers that are inactive in electron transport. – Plant Cell Physiol. **37**: 307-312, 1996.
Tian Z.W., Liu X.X., Gu S.L. *et al.*: Postponed and reduced basal nitrogen application improves nitrogen use efficiency and plant growth of winter wheat. – J. Integr. Agr. **17**: 2648-2661, 2018.
Tikkanen M., Aro E.-M.: Integrative regulatory network of plant thylakoid energy transduction. – Trends Plant Sci. **19**: 10-17, 2014.
Vines H.M., Tu Z.-P., Armitage A.M. *et al.*: Environmental responses of the post-lower illumination CO_2 burst as related to leaf photorespiration. – Plant Physiol. **73**: 25-30, 1983.
Walker B.J., Drewry D.T., Slattery R.A. *et al.*: Chlorophyll can be reduced in crop canopies with little penalty to photosynthesis. – Plant Physiol. **176**: 1215-1232, 2018.
Wang Y., Zheng W., Zheng W.J. *et al.*: Physiological and transcriptomic analyses of a yellow-green mutant with high photosynthetic efficiency in wheat (*Triticum aestivum* L.). – Funct. Integr. Genomic. **18**: 175-194, 2018.
Wingler A., Lea P.J., Quick W.P., Leegood R.C.: Photorespiration: metabolic pathways and their role in stress protection. – Philos. T. Roy. Soc. B **355**: 1517-1529, 2000.
Xiong D.L., Wang D., Liu X. *et al.*: Leaf density explains variation in leaf mass per area in rice between cultivars and nitrogen treatments. – Ann. Bot.-London **117**: 963-971, 2016.
Zhang J.-Y., Cun Z., Chen J.-W.: Photosynthetic performance and photosynthesis-related gene expression coordinated in a shade-tolerant species *Panax notoginseng* under nitrogen regimes. – BMC Plant Biol. **20**: 273, 2020.
Zheng S., Siman G., Tong L. *et al.*: [Effect of nitrogen application rate on growth yield and quality of wheat with different chlorophyll content.] – J. Triticeae Crops **41**: 1134-1142, 2021. [In Chinese]
Zivcak M., Kalaji H.M., Shao H.-B. *et al.*: Photosynthetic proton and electron transport in wheat leaves under prolonged moderate drought stress. – J. Photoch. Photobio. B **137**: 107-115, 2014a.
Zivcak M., Olsovska K., Slamka P. *et al.*: Application of chlorophyll fluorescence performance indices to assess the wheat photosynthetic functions influenced by nitrogen deficiency. – Plant Soil Environ. **60**: 210-215, 2014b.